

de Haas-van Alphen effect in single crystal MgB₂

E. A. Yelland and J. R. Cooper

*Interdisciplinary Research Centre in Superconductivity and Department of Physics,
University of Cambridge, Madingley Road, Cambridge CB3 0HE, United Kingdom.*

A. Carrington, N. E. Hussey and P. J. Meeson

H. H. Wills Physics Laboratory, University of Bristol, Tyndall Avenue, BS8 1TL, United Kingdom.

S. Lee, A. Yamamoto and S. Tajima

Superconductivity Research Laboratory, International Superconducting Technology Center, Tokyo 135-0062, Japan.

(Dated: December 2, 2024)

We report observations of quantum oscillations in single crystals of the high temperature superconductor MgB₂. Three de Haas-van Alphen frequencies are clearly resolved. We propose that two of these come from a single warped Fermi surface tube along the *c* direction, and that the third arises from cylindrical sections of the in-plane honeycomb network. The corresponding effective masses range from $0.44 - 0.68m_e$. Our results show some differences from the calculated band-structure, and should help define key parameters in the theory of superconductivity for this compound.

The discovery of high temperature superconductivity, in MgB₂ [1] has led to great interest in this hexagonal layered compound. Early isotope effect work clearly showed that phonons are important [2], but subsequent experiments and calculations by a number of groups have revealed some unusual features, such as the possible existence of two distinct superconducting gaps [3, 4, 5, 6], that may be associated with two different bands [7]. A central question is whether a conventional phonon mechanism can produce a transition temperature, T_c of 39 K. For microscopic models to answer this, a detailed knowledge of the Fermi surface parameters is required.

Studies of the de Haas-van Alphen (dHvA) effect provide crucial information about the electronic properties of metals and superconductors. Observation of quantum oscillations allows the shape of the Fermi surface and the effective masses of carriers on individual Fermi sheets to be found. Then, together with band-structure calculations, electron-phonon coupling constants can be obtained [8]. Here we report a detailed study of the dHvA effect in single crystals of MgB₂. Three dHvA frequencies are clearly resolved in our data, and can be assigned to two distinct, orthogonal Fermi surfaces parallel to the main symmetry axes of MgB₂. The effective masses of both surfaces are rather small ($0.44 - 0.68m_e$), and preliminary comparison with band-structure calculations [7, 9, 10, 11, 12] reveals some differences.

The single crystals used in this work were grown in Tokyo by high pressure synthesis, as described in Ref. [13]. Two crystals from the same batch were studied in parallel using sensitive piezo-resistive cantilevers to measure the torque (Γ) [14, 15] – crystal A at Cambridge using a ⁴He cryostat with a 15 T magnet and crystal B at Bristol using a ³He cryostat with an 18 T magnet. The dimensions of the crystals A and B were $230 \times 80 \times 20 \mu\text{m}^3$ and $230 \times 200 \times 47 \mu\text{m}^3$ respectively (the shortest side being along the *c*-axis). Thermal contact between the crys-

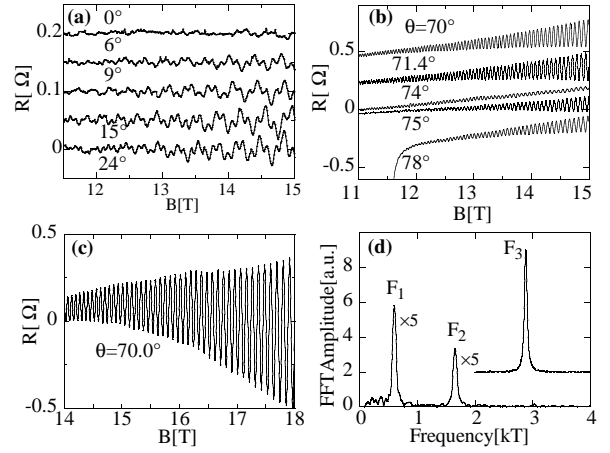


FIG. 1: Panels a-c: dHvA signals at several angles, rotating from [001] to [100]. Panel d: FFTs of the data at $\theta = 20^\circ$ (F_1 and F_2) and 70° (F_3). The top and bottom panels show data for crystals A and B at 1.35 K and 0.36 K, respectively.

tals and nearby calibrated thermometers was ensured by immersion in ³He or ⁴He liquids or a few mbars pressure of exchange gas. Both cryostats had a single-axis low-temperature rotatable sample stage and angles were measured to a relative accuracy of at least 1° . For crystal A, the alignment was verified from the symmetry of high resolution, torque versus angle sweeps near the *c*-axis at 15 T, while for B a correction of 6° was applied to make the dHvA frequencies symmetrical about the crystal axes. The data obtained in both sets of experiments were essentially identical.

Fig. 1 (panels a-c) show torque versus magnetic field data [16] for both crystals as a function of angle, as the crystals were rotated from $B \parallel [001]$ ($\theta = 0^\circ$) to $[100]$ ($\theta = 90^\circ$). Initially, the orientation of the *c*-axis was determined from the platelet shape and the anisotropy

of the upper critical field H_{c2} . As expected, the torque signal goes to zero at the principal symmetry directions ($\theta = 0^\circ$ and 90°) but is already sizable only a few degrees away. The signal was easily resolved over a wide field range, giving well defined dHvA frequencies [see the fast Fourier transforms (FFTs) in Fig. 1 (panel d)]. Two frequencies (F_1 and F_2) were observed for field sweeps carried out within $\sim 45^\circ$ of the c -axis [Fig. 1(a)], while only a single frequency F_3 was found for fields nearer the plane [Fig. 1(b) and (c)].

The dHvA signals were analyzed in the conventional way using the Lifshitz-Kosevich (LK) expression [8, 17] for the oscillatory magnetization of a 3D Fermi liquid

$$M_{osc} \propto B^{\frac{1}{2}} R_D R_T R_S \sin \left(\frac{2\pi F}{B} + \gamma \right) \quad (1)$$

where F is the dHvA frequency [$F = (\hbar/2\pi e)A$, A is the extremal orbit area in \mathbf{k} -space]; γ is the phase; R_D , R_T and R_S are the damping factors from impurity scattering, temperature (T) and spin splitting respectively. $R_D = \exp(-\pi m^B/eB\tau)$, where m^B is the unenhanced or ‘bare’ band mass [8, 17] and τ is the scattering time. $R_T = X/(\sinh X)$ where $X = (m^*/m_e)(14.69/B)T$, and m^* is the quasi-particle effective mass, that is enhanced over m^B by both electron-electron and electron-phonon interactions, and m_e is the free-electron mass. The spin splitting phase factor is given by $R_S = \cos(n\pi g m^S/2m_e)$ where g is the Landé g -factor for electrons in a given orbit, and m^S/m^B is the enhancement of the Pauli susceptibility from electron-electron interactions.

Fig. 2 (upper panel) shows the angular dependence of the three dHvA frequencies observed in both crystals on rotating from $B \parallel [001]$ to $[100]$. There is excellent agreement between the two sets of data. The strong, nearly cosine angular dependence of F_1 and F_2 suggests that they arise from cylindrical sections along the c -axis. The small deviations from a strict $1/\cos\theta$ dependence are shown in inset (a) of Fig. 2. Assuming a simple cosine c -axis dispersion [i.e., $\varepsilon_k = \hbar^2(k_x^2 + k_y^2)/2m - 2t \cos(ck_z)$], Yamaji [18] derived a formula which accounts for the ‘magic-angle’ magnetoresistance maxima in quasi-2D organic superconductors. This gives the angular dependence of the two frequencies, F_{\pm} , arising from extremal areas of a single warped cylinder as,

$$F_{\pm}(\theta) \cos \theta = (\hbar/2\pi e)[\pi k_f^2 \pm 4\pi m t J_0(ck_f \tan \theta)] \quad (2)$$

In this expression, the first term is the mean frequency $(\hbar/2\pi e)\pi k_f^2 = (F_1^0 + F_2^0)/2$, the prefactor of the second term $(\hbar/2\pi e)4\pi m t$ is $(F_2^0 - F_1^0)/2$ and J_0 is the Bessel function. Here F_1^0 and F_2^0 represent F_1 and F_2 at $\theta = 0$, and may be taken directly from the data, so this equation has no free parameters. The good agreement shown in inset (a) of Fig. 2 implies that F_1 and F_2 are the two extremal orbits of a single warped tube. As shown in inset (b), for the other orbit, $F_3 \cos(90 - \theta)$ is remarkably

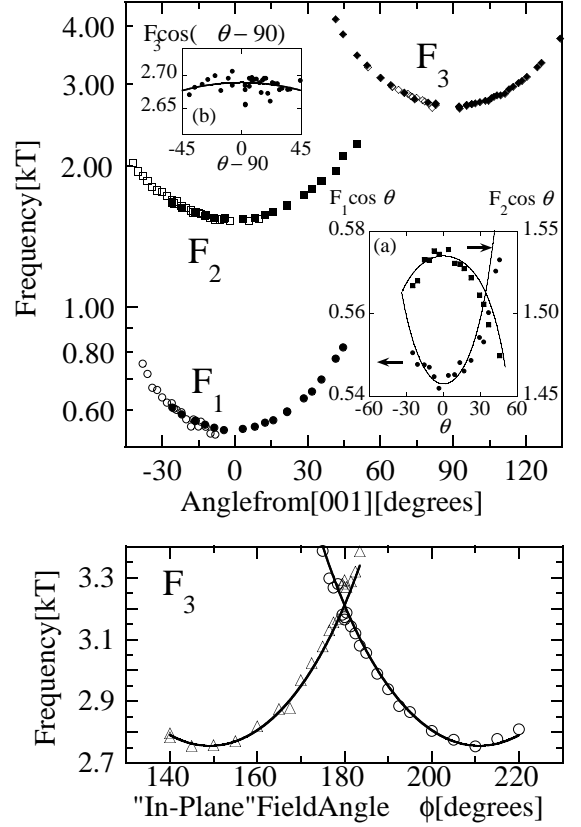


FIG. 2: Upper Panel: Angular dependence of all three frequencies for a rotation between $[001]$ and $[100]$. The open/closed symbols are data for crystals A/B respectively. Inset (a) $F_1 \cos \theta$ and $F_2 \cos \theta$, with a fit to Eq. (2). Inset (b) $F_3 \cos(\theta - 90)$. Lower Panel: In-plane rotation plot for F_3 , crystal A, with fits: $2685/(|\cos \beta \sin \phi| + |\sin \beta \cos 15 \cos \phi|)$ where $\beta = 60$ or 120 .

constant (to within $\pm 1\%$ over $\pm 40^\circ$) implying that it is cylindrical with very little warping.

In Fig. 2 (lower panel), we show results obtained in a second experiment on crystal A in which the c -axis was aligned at $\sim 15^\circ$ from the rotation axis and the magnetic field was rotated approximately within the basal plane. Two minima separated by 60° were observed, consistent with the hexagonal symmetry of MgB_2 . The minimum value of F_3 in the upper panel agrees with that in the lower panel (after correcting for the 15° offset) showing that when $\theta = 90^\circ$, in the upper panel, B lies along the $[100]$ symmetry direction.

Temperature dependent studies were made for all three frequencies from 1.35 K to 12 K (crystal A) and 0.36 K to 12 K (crystal B) and analyzed in the standard way by fitting the data to the damping factor R_T [Eq. (1)]. Fits for crystal B are shown in Fig. 3, and values of m^* obtained in this way for both crystals are given in Table I. Measurements of m^* were made with B approximately 20° off a symmetry axis. The values in Table I have been

TABLE I: Summary of results for both samples.

orbit		F_1^0	F_2^0	F_3^0
Freq. [T]	A	535 \pm 4	1530 \pm 15	2688 \pm 14
	B	546 \pm 1	1533 \pm 10	2685 \pm 2
Mass m^* [m_e]	A	0.53 \pm 0.01	0.680 \pm 0.03	0.446 \pm 0.01
	B	0.553 \pm 0.01	0.648 \pm 0.01	0.441 \pm 0.01
τ [ps], (ℓ [Å])	A	0.18 (600)	0.18 (630)	0.10 (830)
	B	0.14 (414)	0.15 (630)	0.09 (730)

multiplied by $\cos(\theta)$ [or $\sin(\theta)$] to correct for the usual angular dependence of the mass for a tubular band. This correction is less than 8%.

In the inset to Fig. 3 we show the angular dependence of the dHvA amplitude near [100], for both crystals. There is a pronounced dip between 14° and 18° . The slight difference for the two crystals is ascribed to small alignment errors in the direction perpendicular to the axis of rotation. No such dip was observed for F_1 and F_2 . We believe the dip for F_3 is a ‘spin-zero’, which is often observed in dHvA studies when the areas of spin-up and spin-down extremal orbits differ by a half-integral number of Landau quanta, leading to destructive interference in the oscillatory magnetization. This dip was shown to persist to at least 4.2 K. Since F_3 comes from a tubular surface, whose effective area $\propto 1/\cos\theta$, it is easily shown that such zeros occur at angles θ_{sz} given by $g\frac{m^S}{m_e} = n\cos\theta_{sz}$, with $n = 1, 3, 5, \dots$. As before, $\frac{m^S}{m_e}$

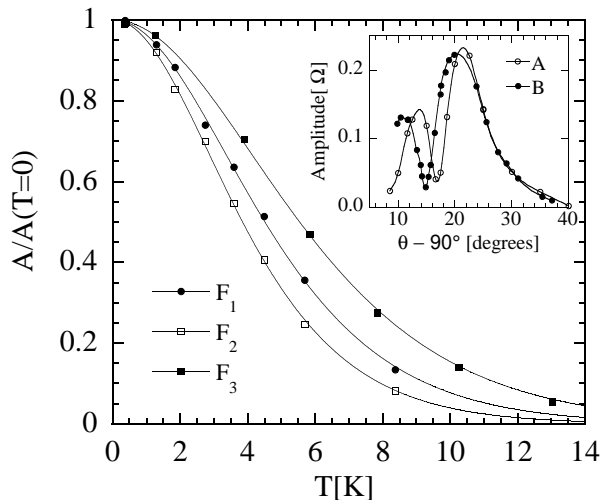


FIG. 3: Dependence of dHvA amplitude on temperature. The amplitude was measured by fitting the sine function [Eq. (1)] to 1.5 oscillations in the range $17.70 \rightarrow 17.82$ T for F_3 and $16.6 \rightarrow 17.9$ T for F_1 and F_2 . The field was determined as the mean of $1/B$ in this window. The fit is to R_T in Eq. (1). Inset: Dependence of amplitude on angle for θ near [100] for crystals A (○) and B (●). Raw data are shown for A at 15 T and 1.35 K [16] with data for B at 18 T and 0.36 K, normalized to the same peak height.

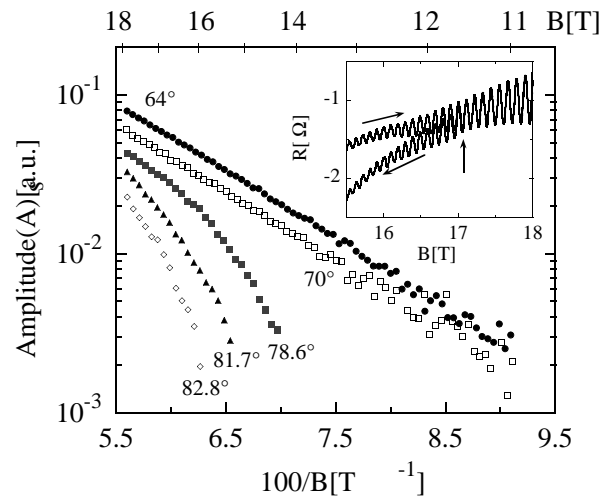


FIG. 4: dHvA amplitude (A_s) at 0.36 K versus inverse field for several values of θ . The inset shows up and down field sweeps at 81.7° . The field sweep direction is indicated. The vertical arrow marks the point where the hysteresis vanishes.

includes band effects and electron-electron enhancement but not electron-phonon enhancement of the standard type [8]. This is because the Pauli susceptibility of a metal can be enhanced by electron-electron interactions, e.g., by the Stoner mechanism, but not by the electron-phonon interaction. Our data give $\theta_{sz} = 18 \pm 3^\circ$, and for $n = 1$ this gives $gm^S/2 = 0.476 \pm 0.007m_e$. Recent conduction electron spin resonance work [19] shows that the average g -factor of MgB_2 is very close to 2.00. Since F_3 arises from a large part of the Fermi surface, it is very likely that $g = 2$ for this band, giving $m^S = 0.476 \pm 0.007m_e$. We see that m^S is close to the dHvA mass determined from the T dependence of the dHvA amplitude [$m^* = 0.441 \pm 0.01m_e$ (Table I)]. This is a curious and potentially important result, given that we expect m^* to be substantially enhanced by the electron-phonon interaction.

The scattering rates of the three orbits were extracted using two procedures. We either subtracted a smoothly varying background and fitted the whole field sweep to Eq. (1) (or more precisely, $\Gamma \propto BM_{osc} \partial \ln F / \partial \theta$), or fitted Eq. (1) to 1.5 oscillations in $1/B$ to give the dHvA amplitude with the thermal damping factor removed (A_s), as a function of B . In both cases we used the values of m^* from Table I in the R_T factor and set $R_S = 1$. In field regions where the sample is clearly in the normal state, the first method gives excellent agreement with Eq. (1) for all three frequencies. Scattering times derived from fits for both crystals and all frequencies are shown in Table I. Making the approximation that all three frequencies arise from circular areas in \mathbf{k} -space, we can obtain k_F for each area and hence $v_F = \hbar k_F / m^*$, and the mean free path $\ell = v_F \tau$. These are also shown in Table I. Similarly we can make approximate estimates

of the Fermi energy of each surface relative to the bottom of the band (these could be up to a factor η (> 1) too low if the values of m^* in Table I are enhanced by a factor η because of interactions). The corresponding values are 1270, 3045 and 7700 K respectively for F_1 , F_2 and F_3 .

The second procedure removes thermal damping effects and reveals changes in the amplitude (A_s) versus $1/B$ plots caused by the onset of superconductivity below H_{c2} . As shown in Fig. 4 at angles of 70° or less, the usual exponential behavior is obtained, (with slopes $\propto 1/\cos(90 - \theta)$ as expected for a tubular surface). However, for angles nearer to the plane, the Dingle plots become non-linear because of additional damping caused by the growth of the superconducting gap, as has been observed in many superconductors (see for example Ref. [20]). This observation proves that our dHvA signals arise from MgB_2 rather than any impurity phase. The inset to Fig. 4 shows hysteresis arising from superconductivity that roughly corresponds to the onset of non-linearity in the Dingle plot. However, the slope of the Dingle plot for $\theta = 81.7^\circ$ remains high above 17 T, suggesting that the superconductivity has not been entirely suppressed in the reversible region. A detailed analysis of the dHvA data in the superconducting state will be reported later.

Band-structure calculations for MgB_2 have been made by several groups (e.g., [9, 11, 12]), including dHvA frequencies and masses for B along the c -axis [10]. The calculated Fermi surface has two small warped cylinders along the c -direction, and two sheets of tubular networks in the basal plane. Comparison with our experimental data suggests that F_1 and F_2 arise from the inner c -axis cylinder, but our frequencies are a factor of 1.8 (F_1) and 1.4 (F_2) smaller than theory [10]. The size and symmetry of F_3 seem to correspond to uniform sections of the electron-like tubular network, whose median plane contains the A, H and L symmetry points [9], but the measured value of F_3 is a factor of 1.4 lower than that estimated from Fig. 3 of Ref. [9]. Because of the discrepancies in the frequencies, estimates of electron-phonon enhancement factors, using our values of m^* (Table I) will await refined bandstructure calculations.

The absence of other orbits in our study could be due to a number of factors. The damping factor R_D in Eq. (1) is exponentially dependent on the ratio m^B/τ which varies as ℓ^{-1} . Based on our experimental signal to noise ratio, we estimate that surfaces with larger values of m^B should be detectable provided that m^B/τ is not more than two times larger than our present values. This is an upper limit because we have not included the effects of the band curvature factor in the LK expression [8], or the fact that torque signal is only large for orbits whose area changes markedly with angle. However, from the mass estimates in Ref. [10] we would expect to see at least the second c -axis orientated cylinder, (unless ℓ is a factor of ~ 2 smaller on this surface) and so it is possible that this

band is absent, as has been predicted recently [21].

In summary we have presented dHvA data for two single crystals of the new superconductor MgB_2 . The two sets of data are in excellent agreement. There are differences with band-structure calculations that could have important implications for microscopic models of superconductivity in MgB_2 .

JRC is grateful to D. E. Farrell for introducing him to the cantilever technique during a sabbatical year in Cambridge in 1997 and to J. W. Loram and W. Y. Liang for their support. We thank S. M. Hayden, J. Kortus, M. Springford, G. Santi, and J. A. Wilson for helpful discussions. This work was supported by the NEDO (Japan) as Collaborative Research and Development of Fundamental Technologies for Superconductivity Applications and the EPSRC (U.K.). PJM gratefully acknowledges the support of the Royal Society (London).

Note added: Since the original submission of this paper calculations of dHvA frequencies and band masses have been reported independently by three groups [22, 23, 24]. They all show agreement with our frequencies at the level of ~ 300 T or about 1% in k_f/a^* . Their band masses can now be compared with our values of m^* to determine the electron-phonon enhancement factors (λ), giving $\lambda = 1.26, 1.08$ and 0.40 for the three orbits F_1, F_2 and F_3 respectively. The latter also agree with the calculated values, 1.25, 1.25 and 0.47 [7, 23]. Therefore the present work provides direct experimental evidence in favor of the microscopic two-band theory of superconductivity in MgB_2 [7].

-
- [1] J. Nagamatsu, N. Nakagawa, T. Muranaka, Y. Zenitani and J. Akimitsu, *Nature* **410**, 63 (2001).
 - [2] S.L. Bud'ko *et al.*, *Phys. Rev. Lett.* **86**, 1877 (2001).
 - [3] F. Bouquet *et al.*, *EuroPhys. Lett.* **56**, 856 (2001).
 - [4] X.K. Chen, M.J. Konstantinović, J.C. Irwin, D.D. Lawrie and J.P. Franck, *Phys. Rev. Lett.* **87**, 157002 (2001).
 - [5] P. Szabó *et al.*, *Phys. Rev. Lett.* **87**, 137005 (2001).
 - [6] F. Manzano, A. Carrington, N.E. Hussey, S. Lee, A. Yamamoto, S. Tajima, *Phys. Rev. Lett.* **88**, 047002 (2002).
 - [7] A.Y. Liu, I.I. Mazin and J. Kortus, *Phys. Rev. Lett.* **87**, 087005 (2001).
 - [8] D. Shoenberg, *Magnetic Oscillations in Metals*, (Cambridge University Press, 1984). ISBN 0521 224802
 - [9] J. Kortus, I.I. Mazin, K.D. Belashchenko, *Phys. Rev. Lett.* **86**, 4656 (2001).
 - [10] S. Elgazzar, P. M. Oppeneer, S.-L. Drechsler, R. Hayn and H. Rosner, *Solid State Comms.*, **121**, 99, (2002)
 - [11] S.V. Shulga, S.-L. Drechsler, H. Eschrig, H. Rosner and W.E. Pickett, *cond-mat/0103154*.
 - [12] G. Santi *et al.*, (Unpublished).
 - [13] S. Lee, H. Mori, T. Masui, Y. Eltsev, A. Yamamoto and S. Tajima, *J. Phys. Soc. Japan* **70**, 2255 (2001).
 - [14] C. Lupien, B. Ellman, P. Grütter and L. Taillefer, *Appl. Phys. Lett.* **74**, 451 (1999).
 - [15] C. Bergemann, Ph.D. Thesis (University of Cambridge)

- (1999).
- [16] Typical noise levels were $\pm 8 \text{ m}\Omega$ (sample A) and $\pm 4 \text{ m}\Omega$ (sample B) in the $2300 \text{ }\Omega$ piezolever resistance, corresponding to $\pm 2 \times 10^{-13} \text{ Nm}$ in the torque. The conversion factor for the Wheatstone bridge data in Figs. 1 and 3(insert) is $\approx 10^{-10} \text{ Nm}/\Omega$. Low field measurements in the diamagnetic state showed that this factor changed by less than $\pm 5 \%$ between 1.4 K and 10 K
 - [17] A. Wasserman and M.S. Springford, Adv. Phys. **45**, 471 (1996).
 - [18] K. Yamaji, J. Phys. Soc. Japan **58**, 1520 (1989).
 - [19] F. Simon *et al.*, Phys. Rev. Lett. **87**, 047002 (2001).
 - [20] T.J.B.M. Janssen, C. Haworth, S.M. Hayden, P.J. Meeson and M. Springford, Phys. Rev. B **57**, 11698 (1998).
 - [21] L. Boeri, G.B. Bachelet, E. Cappelluti and L. Pietronero, condmat/0112075.
 - [22] H. Harima, *International Symposium on Superconductivity 2001, Kobe, Japan* (Proceedings to appear in Physica C).
 - [23] I.I. Mazin and J. Kortus, cond-mat/0201247
 - [24] S. Elgazzar, P.M. Oppeneer, S.-L. Drechsler, R. Hayn, and H. Rosner, cond-mat/0201230